**EPJ manuscript No.**
(will be inserted by the editor)

# Relationship between vibrations and dynamical heterogeneity in a model glass former: extended soft modes but local relaxation

Douglas J. Ashton[1,2] and Juan P. Garrahan[1]

[1] School of Physics and Astronomy, University of Nottingham, Nottingham, NG7 2RD, U.K.
[2] Department of Physics, University of Bath, Bath, BA2 7AY, U.K.

Received: date / Revised version: date

**Abstract.** We study the relation between short-time vibrational modes and long-time relaxational dynamics in a kinetically constrained lattice gas with harmonic interactions between neighbouring particles. We find a correlation between the location of the low (high) frequency vibrational modes and regions of high (low) propensity for motion. This is similar to what was observed in continuous force systems, but our interpretation is different: in our case relaxation is due to localised excitations which propagate through the system; these localised excitations act as background disorder for the elastic network, giving rise to anomalous vibrational modes. Our results provide an example whereby a correlation between spatially extended low frequency modes and high propensity regions does not imply that relaxational dynamics originates in extended soft modes but rather belies their common origin. We consider other measures of elastic heterogeneity, such as non-affine displacement fields and mode localisation lengths, and discuss implications of our results to interpretations of dynamic heterogeneity more generally.

**PACS.** 64.70.Q- Theory and modelling of the glass transition – 63.50.Lm Vibrational states in glasses and amorphous solids – 83.80.Ab Rheology of glasses

## 1 Introduction

Two of the central features of glass forming systems are, on the one hand, the increasingly fluctuating, heterogenous dynamics [1] that accompanies the growth of relaxational timescales in supercooled liquids [2], and on the other, the anomalies in their vibrational spectrum when considered as amorphous solids [3,4]. While the former pertains to structural relaxation on long times (say of the order of seconds for a liquid near the experimental glass transition temperature), and the latter to vibrational motion at high frequency (say in the THz for the Boson peak [3] of glasses), an important question is whether these two characteristic aspects of the dynamics of glass formers are related, and in particular whether there is a common structural origin for both of them.

Interesting recent studies of systems of hard spheres [5], hard disks [6], and soft disks [7] have revealed that the spatial localization of the anomalous low frequency modes of vibrations around either coarse-grained configurations in meta-basins [5,6], or around inherent-structures [7], give a good indication of the spatial distribution of structural relaxation at much longer times. It has been argued [5,6] that this correspondence is causal [7], in that it is these soft vibrational modes which provide the underlying structural mechanism to long time relaxation.

In this paper we address this problem by studying spatial correlation between structural relaxation and vibrational modes in suitably generalized kinetically constrained models of glasses [8]. Our main results are illustrated in Fig. 1. The top left panel is a"propensity" map [9,13] of a two-vacancy assisted lattice gas, or (2)-TLG [10], showing the average spatial distribution of structural relaxation starting from a typical configuration (details are given below). The right hand panels show the location of the lowest frequency modes (top) and highest frequency modes (bottom) of the elastic network obtained from the same configuration when neighbouring particles interact via harmonic springs. There is a clear spatial correlation between low frequency modes and high propensity for relaxation, and high frequency modes and low propensity for relaxation, as in atomistic models [5–7]. Similarly, we find that structural relaxation occurs predominantly along the direction of the low frequency modes [5,6]. In our model, however, relaxation is via the propagation of localized clusters of vacancies [11–13], and does not emanate from the soft vibrational modes. In fact, it is precisely the presence of these localized defects in the elastic network that gives rise to the anomalous soft modes. We conclude that soft vibrational modes do indeed provide a good indicator of long time dynamic heterogeneity, but this correlation does not necessarily imply they are the un-

*Send offprint requests to*:

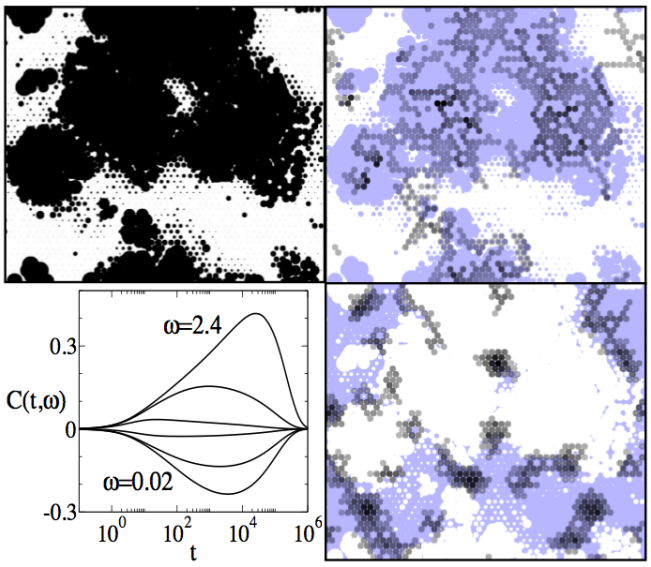


**Fig. 1.** Clockwise from top left: (a) Propensity map of the (2)-TLG at density $\rho = 0.75$ averaged over 100 trajectories. Black circles indicate the isoconfigurational average distance travelled after time $t = 5 \times 10^3$. (b) The average participation, $\nu_i(\omega)$ of the lowest frequency modes, $\omega < 0.1$, and (c) the highest frequency modes, $\omega > 2.4$, of the central force network. (d) The connected correlation, $C(t, \omega)$, between isoconfigurational persistence, $p_i^{\mathrm{IC}}(t)$, and the participation, $\nu_i(\omega)$, as defined in the text. From bottom to top the frequencies are $\omega = 0.02, 0.1, 1, 2, 2.3, 2.4$.

derlying mechanism for long time relaxational dynamics in glass formers in general.

## 2 Models

### 2.1 Glassy dynamics

The models we study are a generalization of constrained lattice gases, first introduced as models of glasses in Ref. [14]. In these models hard-core particles occupy the vertices of a lattice, with single occupancy per site, and with no static interactions between them. For the dynamics, particles try to hop to neighboring sites, but the local hopping rates depend on the occupancy of surrounding sites, so as to mimic steric interactions. These models have the trivial thermodynamics of a non-interacting lattice gas, but their dynamics at high densities displays many of the features of glass formers, such as non-exponential relaxation [14,11], dynamic heterogeneity [12], transport decoupling [12], and aging [15] (see Ref. [8] for a review).

In particular, we focus on the two-vacancy assisted lattice gas model on the triangular lattice [10], or (2)-TLG, where the kinetic constraint is explicitly due to steric restrictions: a particle can hop to an empty nearest neighbour site only if the common two neighbouring sites are also empty. We also consider its three dimensional variant on an FCC lattice, where the constraint is that the four

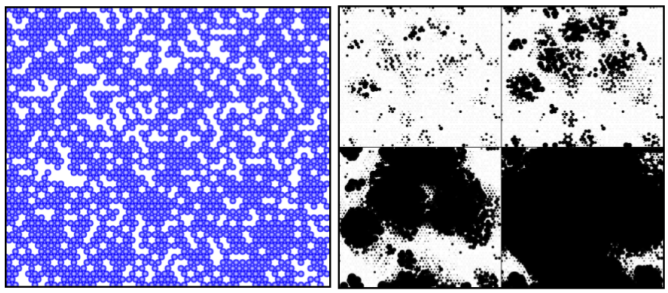

**Fig. 2.** Propensity maps for a (2)-TLG at density $\rho = 0.75$ (second to fifth panels) for the same configuration as Fig. 1 (shown on the leftmost panel) averaged over 100 trajectories. Black circles indicate the average distance travelled by each particle after time, from left to right, $t = 5 \times 10^1, 5 \times 10^2, 5 \times 10^3, 5 \times 10^4$. At this density, $\tau_\alpha \approx 10^4$.

common neighbours of the sites undergoing the transition are empty. We call this model the (4)-FLG [16].

Figure 2 shows propensity maps for the (2)-TLG, which illustrate the spatial localization of relaxational dynamics in the model. The leftmost panel is a typical configuration of the model at a density, $\rho = 0.75$ in this case, for which relaxation is highly non-exponential and heterogeneous [12]. Panels two to five show the average particle displacement at increasing times in the so-called isoconfigurational ensemble [9], i.e., for all trajectories starting from the same initial configuration (the one in the leftmost panel). For a detailed study of propensity in the (2)-TLG model see Ref. [13].

### 2.2 Vibrations

In order to study vibrations together with dynamical heterogeneity we generalize the models above by adding harmonic interactions between neighboring particles. That is, any two occupied nearest neighbor sites interact through a linear spring of force constant $k$ and of rest length equal to the lattice spacing. The vibrational Hamiltonian then reads,

$$H_{\mathrm{vib}} = \sum_{\langle ij \rangle} \frac{1}{2} n_i n_j k \left[ (\delta \boldsymbol{r}_i - \delta \boldsymbol{r}_j) \cdot \hat{r}_{ij}^0 \right]^2 , \qquad (1)$$

where $\langle ij \rangle$ means that the sum is over nearest neighbor pairs, $n_i = 0, 1$ indicates whether lattice site $i$ is empty or occupied, $\delta \boldsymbol{r}_i$ is the displacement of the particle whose equilibrium position is site $i$, and $\hat{r}_{ij}^0$ is the unit vector between sites $i$ and $j$. Each configuration thus gives rise to a disordered elastic network due to the presence of vacancies in the particle configuration. This elastic problem is well known, as it corresponds to the "central force" problem of rigidity percolation [17]. In particular, Eq. (1) for the (2)-TLG and (4)-FLG models correspond to the site diluted triangular and FCC central force networks studied in Ref. [18].

Fig. 3 shows the average density of states (DoS), $D(\omega)$, of vibrational modes for elastic networks corresponding to

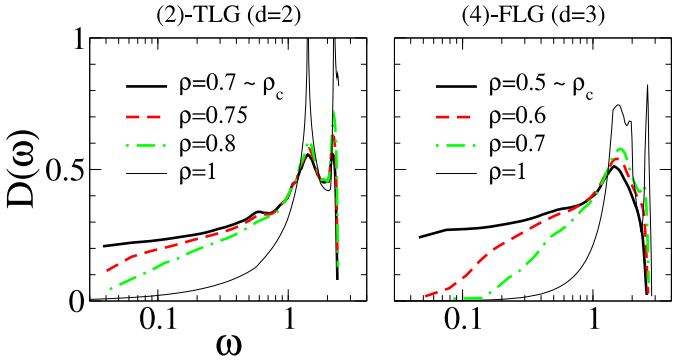


**Fig. 3.** Density of states for the central force networks of the (2)-TLG model (left panel) and the (4)-FLG model (right panel), at various densities $\rho$ above the isostatic density $\rho_c$. The curves at $\rho = 1$ are exact. The curves for all other densities were obtained by numerical diagonalization of the dynamic matrix of systems with 4000 normal modes.

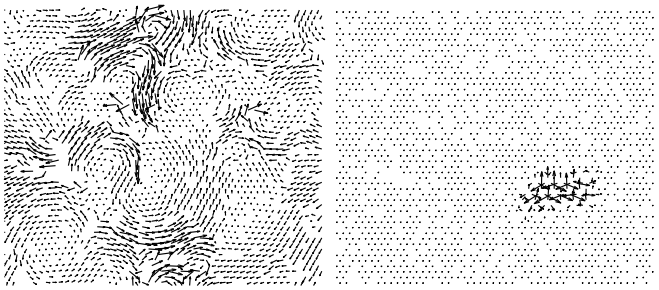

**Fig. 4.** Vector representations of the vibrational modes for the configuration of the (2)-TLG as shown in Fig. 2. Eigenvectors, $\boldsymbol{e}_{i\omega}$, are shown for low frequency, $\omega = 0.054$ (left), and high frequency, $\omega = 2.4$, (right). Low frequency modes are extended with vortex structures while high frequency modes are localised.

the (2)-TLG model and (4)-FLG model at various densities. For densities lower than that of the full lattice, $\rho < 1$, the DoS presents an excess of low frequency modes. Debye scaling, $D(\omega) \propto \omega^{d-1}$, is recovered at low enough frequencies. The presence of excess modes becomes more pronounced as the density decreases. At a critical density, $\rho_c$, the excess tail extends all the way to $\omega = 0$. This is the isostatic point at which the system is marginally rigid [17]. For densities below $\rho_c$ there is an extensive number of zero frequency modes. We find that for the (2)-TLG $\rho_c \approx 0.7$ and for the (4)-FLG $\rho_c \approx 0.5$, which agrees with the results of Ref. [18] for the triangular and FCC lattices, respectively.

For all densities below that of the full lattice, $\rho < 1$, the vibrational modes take on a complex structure. Fig. 4 shows typical examples. The arrow at each occupied lattice site represents the two-dimensional vector, $\boldsymbol{e}_{i\omega}$, which is the $i$-th component of the eigenvector of frequency $\omega$. Low frequency modes are extended with characteristic vortex patterns, while at high frequencies the modes become localised in space. At both high and low frequency the spatial distribution of the modes becomes non-trivial. Figure 1 illustrates this. It shows the spatial weight, $\nu_i(\omega)$, of modes of low frequency (Fig.1, top-right) and high frequency (Fig.1, bottom-right) for the (2)-TLG configuration of Fig. 2, with $\nu_i(\omega) \equiv \boldsymbol{e}_{i\omega} \cdot \boldsymbol{e}_{i\omega}$. With this definition $\sum_i \nu_i(\omega) = 1$ for all $\omega$.

Fig. 1 (top-right) also shows the propensity map for the same configuration (cf. Fig. 2) overlayed on the low frequency eigenvectors. The picture suggests a close correlation between areas of high propensity for relaxational motion and the location of soft modes. Fig. 1 (bottom-right) shows a similar spatial correlation between regions of low propensity (shown as the inverse of Fig. 1, top-left) and the location high frequency modes. In the next section we quantify this correlation and also look at the projection of the particle displacement field directly onto the eigenvectors. Here we find that particles mostly relax along the direction of the low frequency modes. Finally, we discuss further the elastic properties of both the (2)-TLG model and the (4)-FLG model at different densities.

## 3 Results

In order to quantify the correlation between the location of the vibrational modes and the dynamic heterogeneity we define the following cross correlation between local propensity for motion and vibrations:

$$C(t,\omega) = \langle p_i^{\mathrm{IC}}(t)\nu_i(\omega)\rangle - \langle p_i^{\mathrm{IC}}(t)\rangle. \qquad (2)$$

Here $p_i(t)$ denotes the persistence function [12] of particle $i$, i.e. $p_i(t) = 1$ if particle $i$ has not moved up to time $t$, and $p_i(t) = 0$ otherwise. $p_i^{\mathrm{IC}}(t)$ is the iso-configurational average of $p_i(t)$, i.e. the average of the persistence field over all trajectories that start from a given configuration [13]. The average $\langle\cdot\rangle$ in Eq. (2) is over all equilibrium configurations at a given density. Fig. 1 (bottom-left) shows $C(t,\omega)$ as a function of time $t$ for various vibrational frequencies for the (2)-TLG at density $\rho = 0.75$. For high frequencies the correlation is positive, indicating that particles which are more persistent than average also participate in high frequency vibrational modes. For low frequencies the correlation is negative, indicating that fast relaxing particles (low $p_i^{\mathrm{IC}}$) are also those which participate in soft vibrations. In both cases the correlation is non-monotonic in time, peaking at times around $\tau_\alpha$.

Figure 5 shows how the spatial correlation between vibrations and dynamic heterogeneity depends on density. It plots the peak value of $C(t,\omega)$ for vibrational modes of the lowest and highest non-trivial frequencies accessible in the simulations. The fast-relaxation/soft-mode correlation increases with density for all densities larger than the isostatic one, $\rho > \rho_c$. In contrast, the slow-relaxation/high-frequency correlation decreases with increasing density. These trends are similar in dimension two, (2)-TLG, and dimension three, (4)-FLG. Below the isostatic point the correlation between slow regions and low frequency modes changes sign as the vibrational spectrum becomes plagued by zero modes.

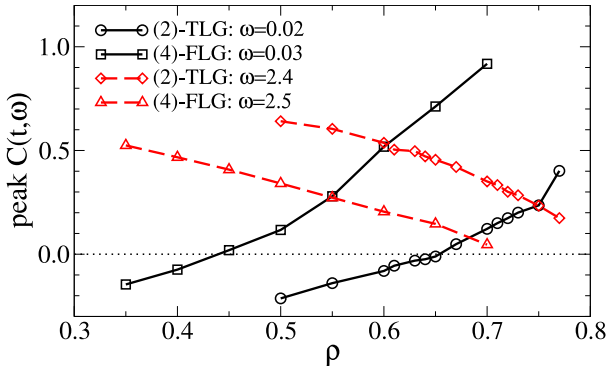


**Fig. 5.** Peak in the absolute value of the correlation $C(t,\omega)$ between propensity for relaxational motion and vibrational modes, in the (2)-TLG and (4)-FLG, as a function of density; cf. Fig. 1 (bottom-left). The correlation between fast regions/high-frequency modes decreases with increasing density. The correlation between slow regions/low-frequency modes increases with increasing density.

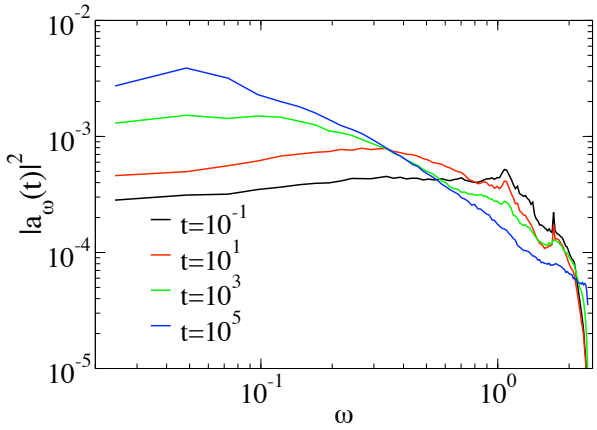


**Fig. 6.** Average projection of the isoconfigurational displacement field, $\delta \boldsymbol{r}_i^{IC}(t)$, on to the vibrational modes, $\boldsymbol{e}_{i\omega}$ (see text) for the (2)-TLG at density $\rho = 0.75$. At early times the projection is evenly distributed. For times around the structural relaxation time, $\tau_\alpha \approx 10^5$, the projection is skewed heavily to low frequencies.

As well as the location of the dynamical heterogeneities, we can also look at their directionality. For this we consider the isoconfigurational average of the particle displacement field, $\delta \boldsymbol{r}_i^{IC}(t) = \boldsymbol{r}_i^{IC}(t) - \boldsymbol{r}_i(0)$. When projected onto the normalized vibrational modes, $\boldsymbol{e}_{i\omega}$, we get projection coefficients

$$a_\omega(t) = \frac{\sum_i \delta \boldsymbol{r}_i^{IC}(t) \cdot \boldsymbol{e}_{i\omega}}{\left(\sum_i |\delta \boldsymbol{r}_i^{IC}(t)|^2\right)^{\frac{1}{2}}} \qquad (3)$$

where the coefficients satisfy $\sum_\omega |a_\omega|^2 = 1$. Fig. 6 shows the projection at four different times for the (2)-TLG at density $\rho = 0.75$. At early times the distribution is flat across the frequency spectrum, with the exception of the highest frequency modes. At later times, around $\tau_\alpha$, the relaxation is occurring mostly along the direction of the low frequency modes. This result is somewhat similar to the findings in studies of hard spheres [5,6] that show the direction of short time relaxation events follow the soft modes. In our case short time relaxation is purely local. However, given enough time, we recover the highly collective motion seen in the low frequency vibrations.

### 3.1 Elastic heterogeneity

The heterogeneity of vibrational modes in the (2)-TLG and (4)-FLG increases with decreasing particle density. This vibrational heterogeneity can be seen by computing the localization length of each mode. We do so by using the method of Ref. [19], where a mode localization length is extracted by tracking the change in its eigenvalue due to asymmetric perturbations of the dynamical matrix [20]. Figure 7 (top) shows the change in the localization length computed in this way for different densities in the (2)-TLG. In the full lattice limit, $\rho = 1$, there are no vibrational anomalies and all the modes are extended. As soon as a small density of vacancies is present some of the modes become localized, as illustrated in Fig. 7 for $\rho = 0.95$. More modes become localized as the density of particles decreases. Near to the isostatic point most modes have localization lengths that are smaller than our system size, see middle panel of Fig. 7 (top). Beyond the isostatic density the system becomes elastically unstable.

Elastic heterogeneity also becomes evident in the non-affine response of our system to an external strain [21, 22]. Following Ref. [22], we deform the system through a uniform strain in the $x$-direction, $\epsilon \ll 1$, by rescaling all particle positions in an affine manner, $\boldsymbol{r}_{i0} \to \boldsymbol{r}'_{i0}$. After the stretch we minimize the energy using conjugate gradient descent. Because of the periodic boundary conditions, once the affine displacement has been made the system will not be able to relax back to its original configuration. The final positions of the particles can be expressed as the sum of an affine part, $\boldsymbol{r}'_{i0}$ and a nonaffine part, $\boldsymbol{u}_i$.

For high densities the conjugate gradient algorithm is very efficient at finding the minimum energy configuration. As density is lowered towards the rigidity threshold the time to converge starts to increase rapidly. This is due to the formation of weakly connected clusters that can make large displacements at a small energy cost. These clusters are the beginnings of the floppy modes that are able to operate almost independently from the rest of the system. At the isostatic point gradient descent cannot converge. To prevent these divergences we have added a small confining harmonic potential of force constant $\Omega$ at each site to Eq. (1). This extra term is diagonal, and so the normal modes remain unchanged but with a shift in frequency.

Figure 7 (bottom) shows the average magnitude of the non-affine response, $\langle (\boldsymbol{u}_i/\epsilon)^2 \rangle^{1/2}$, as a function of the density in the (2)-TLG model. Close to the isostatic point the average non-affine deformation increases very rapidly, and would appear to diverge when $\Omega \to 0$. The inset to Fig. 7

(bottom) has the projection of the non-affine deformation on the normal modes, $\langle u|\omega\rangle \equiv \sum_i \boldsymbol{u}_i \cdot \boldsymbol{e}_{i\omega}$, as a function of frequency of the modes, for the (2)-TLG at density $\rho = 0.75$, showing that non-affinity is carried preferably by softer modes.

## 4 Discussion

We have studied the correlation between dynamic heterogeneity and anomalous vibrations in a two and a three dimensional constrained lattice gas model of glasses. The structural relaxation of these models at high density is similar to that of glass formers, displaying non-exponential relaxation and dynamic heterogeneity [12,13,16]. Their vibrational properties are those of well-studied random networks [18], and mimic characteristic aspects of the anomalous vibrations of glasses: excess low frequency modes, non-affinity and elastic heterogeneity, all related to the presence of an isostatic point.

We have found that the location of anomalous vibrational modes correlates to dynamic heterogeneity of structural relaxation, as is observed in atomistic systems [5–7]. In our case, however, structural relaxation, and therefore dynamic heterogeneity, originate in localized vacancies [11,13], and not in the extended structures that the soft-modes span. In fact, vacancies act as quenched localized defects for the vibrations, cf. Eq. (1), giving rise to the anomalous elastic behaviour observed. We have thus provided a simple example of a system whereby a correlation between soft modes and propensity does necessarily not imply a causal relation for relaxation mechanisms. A similar situation may hold in atomistic models as well.

The authors thank Lester Hedges for discussions. This work was supported by EPSRC grant GR/S54074/01.

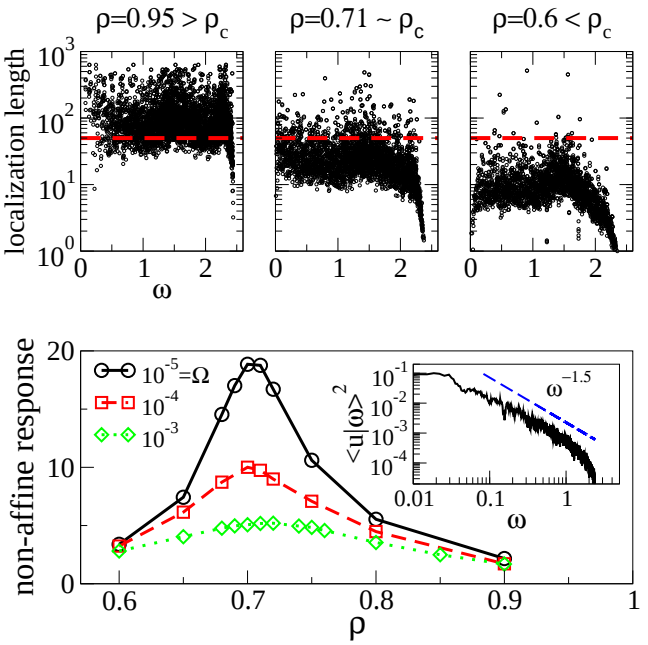


**Fig. 7.** (Top) Localization length of the vibrational modes of the (2)-TLG, calculated using the technique or Ref. [19]. The dashed line indicates the box length, $L = 50$. As the density decreases towards the isostatic point more modes become localized; for densities below the isostatic one the system breaks up into disconnected elastic components. (Bottom) Average non-affine response, $\langle(\boldsymbol{u}_i/\epsilon)^2\rangle^{1/2}$, as a function of density in the (2)-TLG. The different curves are for different strengths $\Omega$ of the confining potential. In the limit of $\Omega \to 0$, the non-affine response appears to diverge at $\rho_c$. Inset: Projection of the non-affine displacement into the vibrational eigenmodes, at $\rho = 0.75$ for $\Omega = 10^{-5}$.

## References


1. For reviews on dynamic heterogeneity see: H. Sillescu, J. Non-Cryst. Solids **243** (1999) 81; M.D. Ediger, Annu. Rev. Phys. Chem. **51** (2000) 99; S.C. Glotzer, J. Non-Cryst. Solids, **274** (2000) 342; R. Richert, J. Phys. Condens. Matter **14** (2002) R703; H. C. Andersen, Proc. Natl. Acad. Sci. U. S. A. **102** (2005) 6686.
2. For reviews on the glass transition see, M.D. Ediger, C.A. Angell and S.R. Nagel, J. Phys. Chem. **100** (1996) 13200; C.A. Angell, Science **267** (1995) 1924; P.G. Debenedetti and F.H. Stillinger, Nature **410** (2001) 259.
3. *Amorphous solids, Low temperature properties*, edited by W.A. Phillips (Springer, Berlin) 1981; C.A. Angell et al., J. Appl. Phys. **88** (2000) 3113; K. Binder and W. Kob in *Glassy Materials and Disordered Solids: An Introduction to their Statistical Mechanics* (World Scientific, Singapore) 2005.
4. See also, L.E. Silbert, A.J. Liu and S.R. Nagel, Phys. Rev. Lett. **95** (2005) 098301 M. Wyart, S.R. Nagel and T.A. Witten T. A., Euro- phys. Lett., **72** (2005) 486.
5. C. Brito and M. Wyart, J. Stat. Mech. (2007) L08003.
6. C. Brito and M. Wyart, arXiv:0804.2439.
7. A. Widmer-Cooper et al., Nature Phys. **4** (2008) 711-715.
8. F. Ritort and P. Sollich, Adv. Phys. **52** (2003) 219.
9. A. Widmer-Cooper, P. Harrowell and H. Fynewever, Phys. Rev. Lett. **93** (2004) 135701.
10. J. Jäckle and A. Krönig, J. Phys. Condens. Matter **6** (1994) 7633.
11. C. Toninelli, G. Biroli and D.S. Fisher, Phys. Rev. Lett. **92** (2004) 185504.
12. A.C. Pan, J.P. Garrahan and D. Chandler, Phys. Rev. E. **72** (2005) 041106.
13. L.O. Hedges and J.P. Garrahan, J. Phys. Condens. Matter **19** (2007) 205124.
14. W. Kob and H.C. Andersen, Phys. Rev. E **48** (1993) 4364.
15. J. Kurchan, L. Peliti and M. Sellito, Europhys. Lett. **39** (1997) 365.
16. D.J. Ashton, PhD Thesis, University of Nottingham, (2008) http://etheses.nottingham.ac.uk/623/.
17. M. F. Thorpe, J. Non-Cryst. Solids **57** (1983) 355; S. Feng and P. N. Sen, Phys. Rev. Lett. **52** (1984) 216; A. Feng, M. F. Thorpe, and E. Garboczi, Phys. Rev. B **31** (1985) 276.
18. M.F. Thorpe and E.J. Garboczi, Phys. Rev. B **35** (1987) 8579.

19. Z. Zeravcic, W. van Saarloos and D.R. Nelson, Europhys. Lett., **83** (2008) 44001.
20. N. Hatano and D.R. Nelson, Phys. Rev. Lett., **77** (1996) 570.
21. B.A. DiDonna and T.C. Lubensky, Phys. Rev. E **72** (2005) 066619.
22. F. Leonforte, A. Tanguy, J.P. Wittmer and J.L. Barrat, Phys. Rev. Lett. **97** (2006) 055501.